ARTICLE

Electrode processes in the KF-AlF_3-Al_2O_3 melt

Sai Krishna Padamata,*[a] Andrey Yasinskiy [a] and Peter Polyakov [a]

Received 00th January 20xx,
Accepted 00th January 20xx

DOI: 10.1039/x0xx00000x

The kinetics of anodic and cathodic processes in KF-AlF_3 and KF-AlF_3-Al_2O_3 melts by the means of stationary polarization and cyclic voltammetry have been studied. Studies were conducted at different cryolite ratios [CR, (moles of KF)/(moles of AlF_3)] and different alumina content between 700–800 °C for Cu-Al anode and at 800 °C for tungsten cathode. The limiting current density of oxygen evolution on Cu-Al anode was 0.31 A cm^{-2} at 700 °C and CR=1.4. It drastically increases with CR and temperature. The limiting current density of aluminium reduction on W cathode was in the range 0.45 – 0.50 A cm^{-2}. The cathodic process is diffusion-controlled while the anodic one shows mixed kinetics. The diffusion and mass transfer coefficients for the cathodic process (W electrode) and the mass transfer coefficient for the anodic process (Cu-Al electrode) were determined. Based on the obtained results, the electrolysis of 1.4KF-AlF_3-Al_2O_3(sat) with Cu-Al anode and W cathode was performed. The aluminium purity was determined with optical emission spectrometer. The XRD, SEM-EDX methods were used to study the phases formed on the anode surface.

1 Introduction

Aluminium is one of the most used metals in the world being only outranked by steel. Global Al production has already reached 64.3 million tons (Mt) for the year 2018 [1]. Being a major greenhouse gas emitting process, aluminium production accounts to 14.4 t of CO_2 evolution (including the indirect emission from the electric power production) per a ton of produced Al [2]. The primary aluminium production has been carried out using the Hall-Heroult process for more than 100 years. Carbon anode and liquid aluminium cathode are used in molten Na_3AlF_6-AlF_3 system at 960-970 °C where aluminium ions are reduced into aluminium. By introducing the additives in the cryolite, the physicochemical parameters like liquidus temperature, viscosity, electrical conductivity and alumina solubility can be modified [3, 4]. The presently used technology for the aluminium reduction is the energy-intensive process responsible for a significant amount of CO_2 and other greenhouse gases in the environment [5, 6]. The following reaction (1) occurs while using carbon anode leading to consumption of the anode and evolution of CO_2 (ΔG^o values here and after are calculated for one mole of aluminium):

$$\frac{3}{2}C_{(s)} + Al_2O_{3(diss)} = 2Al_{(l)} + \frac{3}{2}CO_{2(g)} \quad (1)$$

$\Delta_r G^o$ (960 °C) = 344.793 kJ.mol^{-1} of Al

The search for an oxygen-evolving anode and suitable wettable inert cathode for the aluminium reduction has gained importance for the past few decades due to the increasing pressure on industries to reduce greenhouse gases emission. The reaction (2) takes place while using inert anode:

$$2Al_2O_{3(diss)} = 4Al_{(l)} + 3O_{2(g)} \quad (2)$$

$\Delta_r G^o$ (800 °C) = 668.358 kJ.mol^{-1}

The environmental balance and energy impacts using inert anodes were extensively discussed elsewhere [7-10]. The metallic, cermets and ceramic materials were studied as potential anode materials for aluminium reduction while each has its own advantages and disadvantages [11-18]. Although, metals have shown many promising abilities as they possess high electrical conductivity, thermal shock resistance and ease of fabrication. Moreover, oxide scales formed on the metal anodes protect them from corrosion and improve chemical resistance. With anodic polarization, the metal oxidation occurs according to the reaction:

$$M_{(s)} + xO^{2-}_{(c)} = MO_{x_{(s)}} + 2xe^- \quad (3)$$

Subindex (c) stands for the complex ions. For the reaction (3), the electrochemical potential E is often more negative than the oxygen evolution potential. When the E is greater than 2.2 V (oxygen evolution potential) the anodic reaction is:

$$2O^{2-}_{(c)} = O_{2(g)} + 4e^- \quad (4)$$

[a] 660025, pr. im.g."krasnoyarskiy rabochiy", 95-228. School of non-ferrous metals and materials science, Siberian federal university, Krasnoyarsk, Russia.
* corresponding author. E-mail: saikrishnapadamata17@gmail.com

Reducing the operational temperature of the reduction cell can open the options of using a variety of anode materials. At low operating temperatures, the electrodes possess a low corrosion rate. The low-temperature electrolytes are generally considered as "inert electrodes friendly". The KF-AlF_3 melts come into this category with the working temperature being between 650 and 850 °C depending on the cryolite ratio $\left(\mathrm{CR} = \frac{\text{moles of KF}}{\text{moles of AlF}_3}\right)$ [19]. The eutectic temperature of the NaF-AlF_3 melts used in regular aluminium reduction cell is around 700 °C while for KF-AlF_3 it is only 580 °C [4]. The KF-AlF_3 melts have relatively high alumina solubility [3, 20].

The aluminium bronze (Cu-Al) alloy has been considered as a potential anode material besides Cu-Ni-Fe superalloy. Oxide layer formed on the surface of the anode during the electrolysis process protects the 90Cu-Al anode from corrosion. The CuO, Cu_2O, $CuAlO_2$ and $CuAl_2O_4$ are essential anode oxide layers formed during Al electrolysis [21, 22]. In the alumina-saturated melts, the solubility of Cu_2O is low and it slightly increases with increasing alumina content in the system [23]. According to Feng et al. [24], the oxide layer on the alloy interacts with Al_2O_3 present in the melt leading to the reactions (5-6):

$$\frac{1}{2}\mathrm{Cu_2O} + \frac{1}{2}\mathrm{Al_2O_3} = \mathrm{CuAlO_2} \quad (5)$$

$$\mathrm{Cu} + \frac{1}{2}\mathrm{Al_2O_3} + \frac{1}{4}\mathrm{O_2} = \mathrm{CuAlO_2} \quad (6)$$

From the previous studies [25, 26], it is evident that the reactions (7-8) are expected to occur resulting in the formation of $CuAl_2O_4$:

$$\mathrm{CuO} + \mathrm{Al_2O_3} = \mathrm{CuAl_2O_4} \quad (7)$$

$$\mathrm{Cu} + \mathrm{Al_2O_3} + \frac{1}{2}\mathrm{O_2} = \mathrm{CuAl_2O_4} \quad (8)$$

The aluminium bronze alloy and its oxide layers formed during the oxidation exhibit high electrical conductivity. The high melting point of the alloy can withstand the electrolyte overheating and can be operated without any thermal shocks. Copper aluminates possess low solubility in fluoride salts saturated with O^{2-} ions.

The wettable cathodes are considered as an essential component of the inert electrode system. The cathode process of materials such as liquid aluminium, carbon, graphite, titanium diboride (TiB_2) and tungsten (W) was studied until date [27-35]. W is considered as a model wettable inert cathode. Initially, carbon and graphite cathode process were examined and the results show the Al_4C_3 formation on the cathode surface leads to the passivation and later corrosion of the cathode [36-38]. Although, W forms an intermetallic compound Al_4W with Al interaction on its surface, no significant effect on the kinetic parameters of the cathode process were observed [39,40]. In addition, W shows relatively good chemical resistance towards the liquid aluminium [41]. The electrolysis tests were conducted using aluminium bronze alloy in NaF-KF-AlF_3 system with different proportions [42, 43]. The current efficiency of not more than 77% was achieved and the reduced aluminium contained high contamination of Cu as high as 16.7 wt.%. There was no data available related to the electrolysis test conducted using the inert electrodes (aluminium bronze anode and wettable cathode) at the same time with 1.4 KF-AlF_3-Al_2O_3(sat.). The results would be of interest to the readers who are working towards the development of the inert electrodes.

The article presents the results associated with the kinetics of the anode process on the 90Cu-Al anode in KF-AlF_3-Al_2O_3(sat.) melts between the CR 1.2–1.5 at temperature 700–800 °C. The cathode process of W in KF-AlF_3 melts CR (1.4 and 1.5) at 800 °C was analysed. With kinetic parameters of anode and cathode taking into account, the electrolysis test was performed for 18 hours with vertically placed electrodes [44]. The anode surface was examined using the XRD, SEM-EDX to find the proportions of the different phases in the oxide layer. The current efficiency of the aluminium electrolysis was calculated and the purity of the cathode aluminium was analysed using optical emission spectrometer.

2 Experimental

2.1 Anode preparation

The alloy composed of 90 wt.% of Cu and 10 wt.% of Al was prepared in the vacuum melting furnace at 1050 °C. The material purity was Cu (99.95 %) and Al (99.999%). The equilibrium phase of the Cu-Al system was fcc (∝ Cu-Al) solid solution [45]. The specimens used to determine the kinetics of the anode process were cut in a cylindrical shape with dimension ϕ 15mm × 50 mm for anode process (the geometry of the anode used for electrolysis test varies (see figure 11a)). The specimens were then treated with degreasing agents (ethanol and acetone), dried under air atmosphere before the usage.

2.2 Electrolyte preparation

The KF-AlF_3-based electrolyte was prepared at different CR's according to the requirement from individual KF and AlF_3 salts of reagent grade. Initially, anhydrous KF was dried at 400 °C for 6 hours. The salts with wt.% according to the required CR values were placed in a graphite crucible. The salts were homogeneously mixed in the crucible and heated up to the working temperature. Before determining the characteristics of the electrodes, the electrolyte was refined by using potentiostatic electrolysis method with a graphite working electrode at 0.2 V for 2 hours vs. the Al-electrode potential.

The undesirable impurity residuals in the electrolyte were collected on the graphite electrode.

2.3 Experimental setup and methods

Three-electrode cell was used for electrochemical measurements as shown in figure **1.** The same setup was used to examine the anode and cathode process. The 90Cu-Al cylinder of 15 mm diameter and the tungsten (W) rod of 2 mm diameter were working electrodes used as anode and cathode respectively while determining their parameters. The rest of the electrode surface was protected with a BN tube to have an accurate active surface area. The graphite crucible also acted as a counter electrode. The working electrode potential was measured vs. the Al-reference electrode. The Autolab PGSTAT302n potentiostat with the 20 A booster and Nova 2.1.2 software (The MetrOhm, Netherlands) were used to implement the studies. The temperature of the furnace was maintained constant by using USB-TC01 thermocouple module and measured using Pt/PtRh thermocouple. Stationary state polarisation curves were obtained using chronopotentiograms, where the current was passed for 30 s (at which the potential was attained stationary) and an interrupt of 10 μs was applied. This method helps to obtain cathode potential by eliminating the ohmic drop (IR) from the total potential obtained. The voltammograms for different sweep rates (0.01-0.2 V s^{-1}) were obtained by cyclic voltammetry. The IR was compensated by obtaining the resistance through the I-interrupt method before the start of the cyclic voltammetry. The experiments conducted have temperature fluctuations no more than ± 2°C.

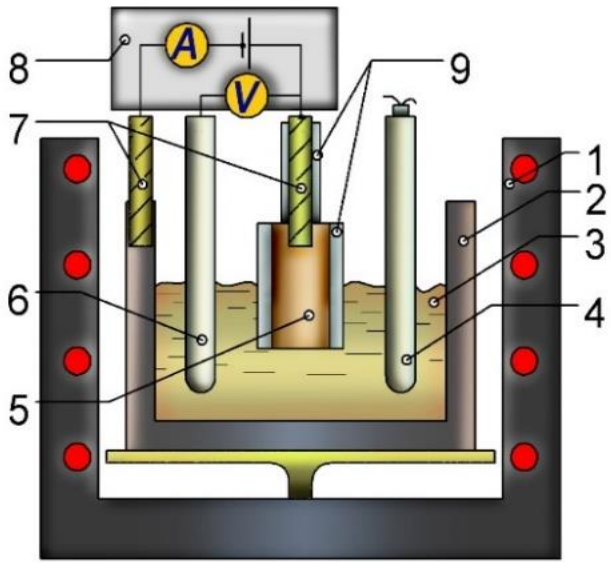

Figure 1. Experimental setup: 1. Vertical electric furnace 2. Graphite crucible 3. Electrolyte 4. k-thermocouple 5. Working electrode 6. Al/AlF_3 reference electrode 7. Steel current lead 8. Potentiostat 9. Boron nitrate tube

2.4 Electrolysis test

Electrolysis test was performing in laboratory two-electrode cell with an amperage of 10 A with 1230 g of the 1.4KF-AlF_3-Al_2O_3(sat) melt. The cell contained graphite crucible with vertically arranged electrodes. The tungsten plate cathode and the 90Cu-Al wt.% anode were used. 212 g of aluminium was placed at the bottom of the crucible, which would collect the aluminium reduced at the cathode. The operating temperature was 800 °C. Al_2O_3 was fed every 30 min for 18 hours and the voltage between the cathode and anode was recorded. The SEM-EDX and XRD analysis were conducted to find the content of the elements on the outer layer of the anode and the anode-melt cross-section. Foundry-Master Pro2 (HITACHI) model optical emission spectrometer was used to find the purity of the cathodic aluminium.

3 Results and discussion

3.1 Anodic process

Stationary galvanostatic polarization of Cu-Al anode was performed over several melts with different cryolite ratios from 1.2 to 1.5 at 700, 750 and 800 °C to study the kinetic parameters of oxygen evolution. The understanding of the current-potential dependences is required for an advance in the search for the corrosion-resistant anode that can be used as an oxygen-evolving electrode in fluoride melts. The anodic current density i_a and the anodic potential E_a (vs. Al reference electrode) were recorded during the experiment. The obtained polarization curves are presented in figure 2.

The curves display several oxidation processes occurred in the range of potentials between 1.8 and 3.5 V. The entire range can be divided into pre-oxygen and oxygen region. Several sections were observed in both regions:

- metal dissolution $\mathrm{Me} + \overset{z\cdot F}{\Rightarrow} \mathrm{Me}^{z+} + \mathrm{ze}^-$
- metal oxidation (ab) $\mathrm{xMe} + \mathrm{yO}^{2-} \overset{2y\cdot F}{\Longrightarrow} \mathrm{Me_xO_y} + 2\mathrm{ye}^-$;
- oxygen ions oxidation (bc) $2\mathrm{O}^{2-} \overset{4F}{\Rightarrow} \mathrm{O}_2 + 4\mathrm{e}^-$;
- apparent oxygen ions oxidation limiting current section (cd) caused by low O^{2-} concentration;
- catastrophic corrosion of the anode.

The oxygen region starts at the potentials 2.3…2.6 V. The oxygen evolution onset potential depends on both CR and T. At high CR and T values this potential was more negative. The oxygen evolution limiting current occurred in cases of low T and low CR. Before that, the anode was oxidized without significant diffusion and kinetic difficulties (ab).

High current densities in the pre-oxygen region of potentials indicate significant dissolution rates of anode oxidation products and a high partial current density of the anode oxidation in the oxygen potential region.

The total anodic overvoltage η_a was found from the polarization curves according to the equation:

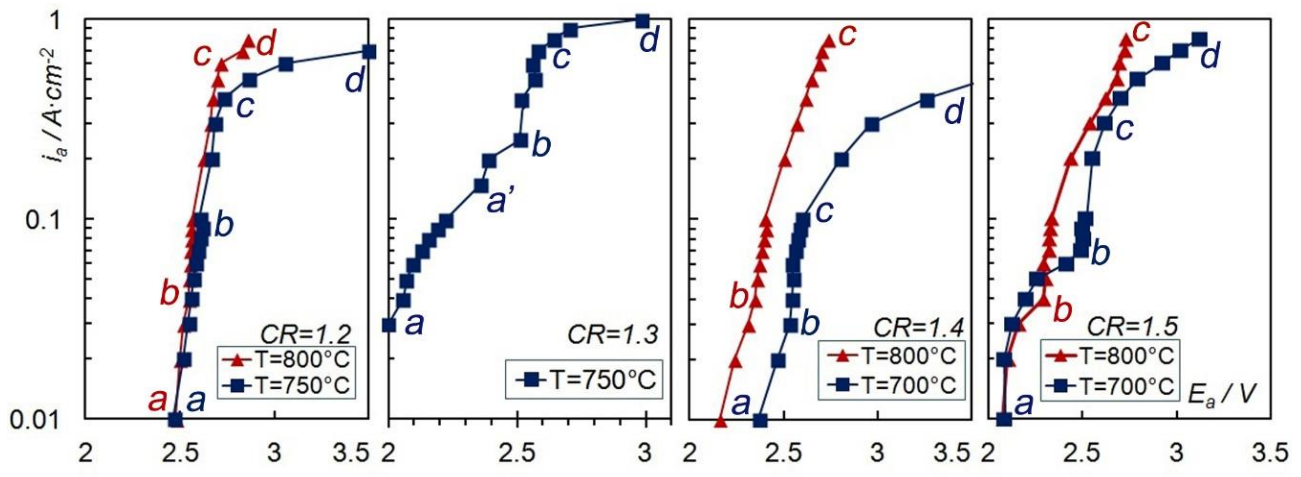

Figure 2. Stationary polarization curves obtained on Cu-Al anode in KF-AlF_3-Al_2O_3 melt at 700, 750 and 800 °C

$$\eta_a = E_i - E_0 \quad (9)$$

where E_i and E_0 are the anodic potential at i A cm^{-2} and the reversible potential respectively.

The ab and bcd sections were treated separately. E_0 for ab process was taken equal to the open circuit potential. E_0 for bcd process was taken equal to the potential in b point. The obtained polarization curves show the mixed kinetics of oxygen evolution. At low current densities, the rate-determining step is a heterogeneous chemical reaction, thus the Tafel equation should be applicable to describe the dependence between activation overvoltage η_{act} and current density:

$$\eta_{act} = \frac{RT}{pzF}\ln i_0 - \frac{RT}{pzF}\ln i \quad (10)$$

where R, T, p, z, F, and i_0 are the gas constant, the temperature, the reaction order, the number of electrons, the Faraday constant and the exchange current density respectively.

After an increase of current density up to a certain value (0.3 A cm^{-2} and higher) diffusion limitations occur, and the concentration overvoltage η_{conc} can be expressed by the following equation:

$$\eta_{conc} = \frac{RT}{zF}\ln\left(1 - \frac{i}{i_l}\right) \quad (11)$$

where i_l is the limiting current density.

For the purpose of the total overvoltage splitting to the activation and concentration components, it was plotted vs. ln i, and the linear section on the graph was considered as activation component of the overvoltage. It was extrapolated to higher values of i. The rest part was considered as the concentration component. The obtained results for CR=1.2 and T=750 and 800 °C are presented in figure 3. The experimental values of the concentration overvoltage η_{conc}(exp.) were estimated with the equation

$$\eta_{conc}(\text{exp.}) = \eta_a - \eta_{act} \quad (12)$$

and were compared with the values calculated according to the equation (11), from which the limiting current density was also found.

The curves (1) and (2) represent the oxidation of metal in the pre-oxygen region of potentials and oxygen evolution respectively. At both temperatures the signs of kinetic and diffusion limitations appear on the oxygen evolution polarization curve. The exchange current density i_0 was found from the extrapolation of the curve linear section to the current density at zero overvoltage. The temperature increase leads to the increase in i_0 from 40 to 74 mA cm^{-2}.

The experimental values of η_{conc} was in a good agreement with the calculated ones for the limiting current density i_l = 0.42 A cm^{-2} at T=750 °C. An increase in T to 800 °C naturally leads to increase in i_l up to 0.72 A cm^{-2}, however there was a appreciable deviation between the experimental and calculated values in certain range of current densities.

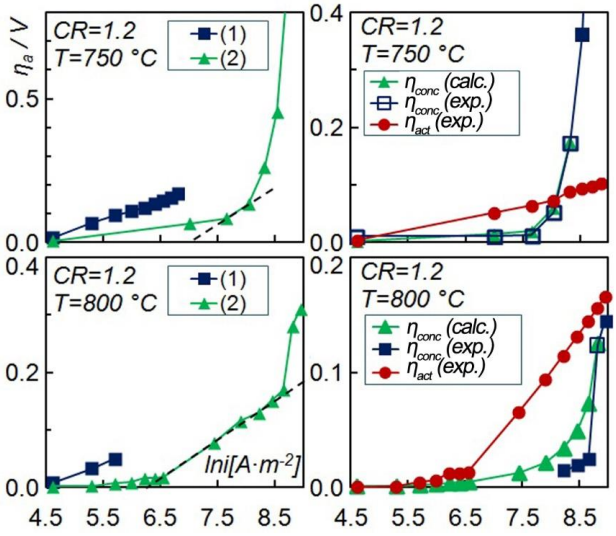

Figure. 3. Dependence of overvoltage vs. partial current density of anode oxidation (1) and oxygen evolution (2); and different kinds of overvoltage (concentration and activation) for oxygen evolution in 1.2KF-AlF_3-Al_2O_3 melt at 750 and 800 °C

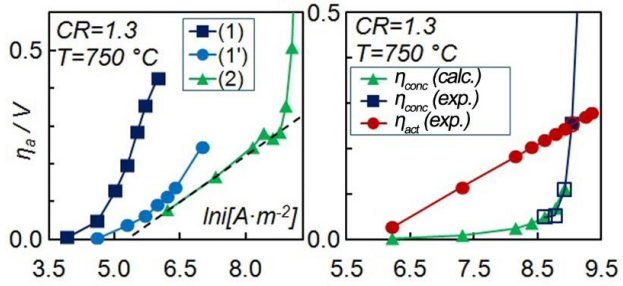

Figure 6. Dependence of overvoltage vs. partial current density of anode oxidation (1) and (1') and oxygen evolution (2); and different kinds of overvoltage (concentration and activation) for oxygen evolution in 1.3KF-AlF_3-Al_2O_3 melt at 750 °C

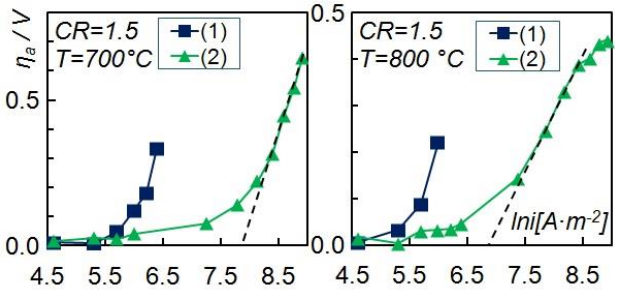

Figure 5. Dependence of overvoltage vs. partial current density of anode oxidation (1) and oxygen evolution (2); in 1.5KF-AlF_3-Al_2O_3 melt at 700 and 800 °C

The reaction order p for heterogeneous chemical reaction was also calculated from the equation (2). The values for T=750 and 800 °C were as high as 1.20 and 0.65 respectively that shows a considerable change in the reaction mechanism.

The same calculations were performed at CR=1.3, 1.4 and 1.5. The results are presented in figures 4, 5, and 6.

There are two different processes observed in the pre-oxygen region of potentials [(1) and (1')] at CR=1.3 and T=750 °C. The first one started from onset potential below 2 V, and the second one started between 2.3 and 2.4 V. Both processes occurred with a significant overvoltage and the rates were determined by the heterogeneous chemical reactions with low reaction orders according to the curve shapes. Oxygen evolution proceeded with mixed kinetics with i_0, p and i_l equal to 36 mA cm^{-2}, 0.55 and 0.82 A cm^{-2} respectively.

Increase in CR to 1.4 led to the appreciable increase in the limiting current density at 800 °C, therefore, it was not observed in the studied ranges of current densities. A decrease in T down to 700 °C resulted in a significant increase in diffusion limitations of the process rate according to the obtained i_l value equal to 0.31 A cm^{-2}. Both T and CR also affected the kinetic parameters of a chemical reaction. The values of i_0 and p were 52 mA cm^{-2} and 0.20 at 700 °C. The same parameters were 49 mA cm^{-2} and 0.33 at 800 °C.

A further increase in CR led to an appreciable increase in i_l. It was not detected even at T=700 °C in the studied range of current densities. A certain deviation from linearity of the curve occurred at i>0.4 A cm^{-2}, which can be connected with the process involving the fluorine ions discharge with the formation of copper fluorides.

Mass transfer coefficient k_s was calculated with the obtained data according to the equation [46]

$$k_s = \frac{i_l}{zFC} \quad (13)$$

where C is the concentration of O^{2-} ions calculated from the alumina solubility, z = 2 All the obtained information is presented in Table 1.

It is shown that i_l naturally increases with an increase in temperature and CR. The effect of CR is associated with the alumina solubility. The mass transfer coefficients for oxygen ions are in the range of (0.5-1.6)·10^{-4} cm s^{-1}. The kinetic parameters of a heterogeneous chemical reaction are also affected by CR and T. The reaction order is higher at lower CR. In most cases, the reaction order is increased with temperature. The exception was observed at CR=1.2 where the value for T=750 °C was rather high, which may be due to the experimental error.

The obtained data for anodic kinetic parameters show that a decrease in the temperature, which is desired to increase the resistivity of anode towards corrosion, leads to the significant drop in mass transfer coefficient for the transport of complex oxygen ions to the anode. The solubility of alumina also highly affects the achievable total anodic overvoltage. The beneficial temperature for the industrial process should not be less than 800 °C. The recommended CR should be 1.4 as it is known [39] that higher values are not favourable with respect to the cathodic process of aluminium reduction.

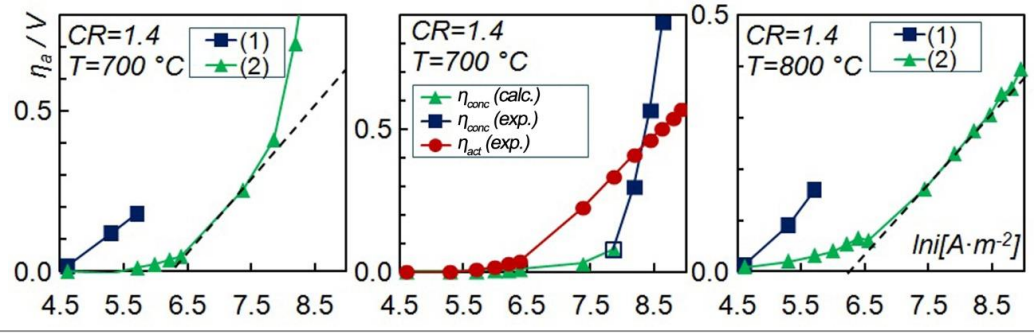

Figure 4. Dependence of overvoltage vs. partial current density of anode oxidation (1) and oxygen evolution (2); and different kinds of overvoltage (concentration and activation) for oxygen evolution in 1.4KF-AlF_3-Al_2O_3 melt at 700 and 800 °C

Table 1. Kinetic parameters of oxygen evolution

CR	T, °C	c·10^2, mole cm^{-3}	i_l, A cm^{-2}	i_0, mA cm^{-2}	k_s·104, cm s^{-1}	p
1.2	750	2.61	0.42	40	0.833	1.20
1.3	750	2.70	0.82	36	1.57	0.55
1.4	700	2.75	0.31	52	0.583	0.20
1.5	700	2.72	n/a	237	n/a	0.08
1.2	800	2.76	0.72	74	1.350	0.65
1.4	800	2.86	n/a	49	n/a	0.33
1.5	800	2.94	n/a	102	n/a	0.20

*concentration of O^{2-} ions was estimated according to the alumina solubility presented in [47]

3.2 Cathodic process

3.2.1 Voltammetry. A typical cyclic voltammograms (CV) obtained on W in $KF - AlF_3$ melts at 800°C are shown in figure 7. The CR values are from 1.3 to 1.5 and the potential sweep rates (v) from 0.01 to 0.2 V.s^{-1}. The cathode peaks associated with the aluminium reduction (Al) depending on the CR values and potential sweep rate can be observed between -0.125 and -0.240 V (vs. Al) for all the CR values. The wave following the cathode peak is related to the potassium (K) reduction.

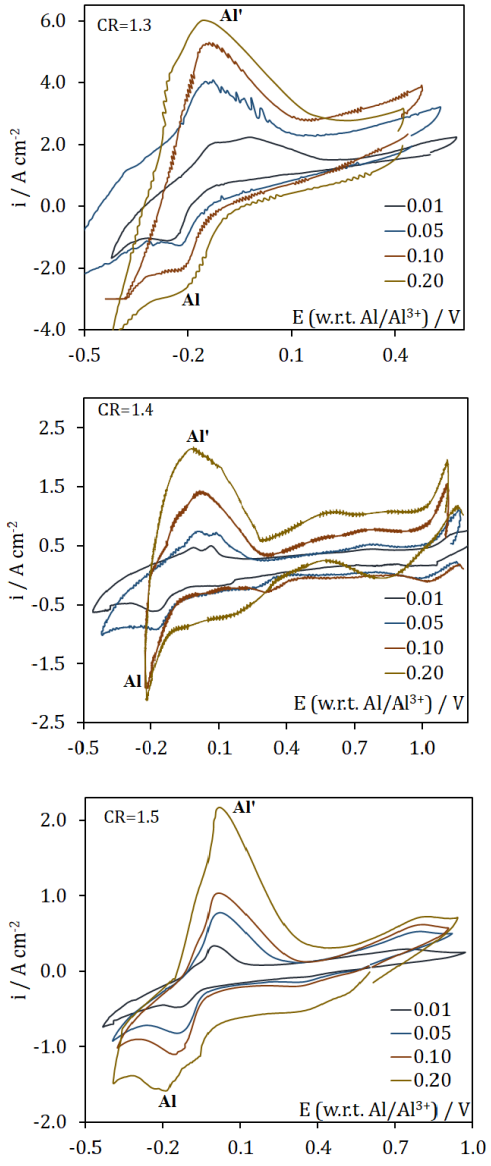

Figure 7. CVs obtained on W electrode at 800 °C for KF-AlF_3 melts (CR = 1.3 to 1.5), potential sweep rates (v) 0.01-0.20 V s^{-1}

The oxidation of the cathode products happens at the anodic peaks (Al'). The anodic peaks occur in the range of -0.14 to -0.07 V. Hugely varying anodic peaks indicate the oxidation of different forms of reduced aluminium in cathode process. Most certainly parallel reactions occur while the aluminium deposition takes place on the cathode surface. Reactions (14-16) occur indefinitely as the melts used are with 0.1 wt.% alumina content. These reactions influence the kinetics of the process to an extent. No visible peaks were observed on voltammogram with a scan rate of 0.2 V/s for 1.4 CR. The reason might be the mixed kinetics involving the reduction of potassium.

$$AlF_4^- + 2e^- = AlF + 3F^- \quad (14)$$

$$AlF_4^- + 3e^- = Al + 4F^- \quad (15)$$

$$Al_2O_2F_4^{2-} + 2AlF_4^- = 2Al_2OF_6^{2-} \quad (16)$$

With the decrease in the CR, the cathode peak current (i_{cp}) increases, stating a significant role in the kinetics of the cathode process. This effect might be due to the increase in the CR values near the cathode layer and consumption of aluminium ions during the electrolysis process. As due to these phenomena, the liquidus temperature near the cathode and melt viscosity increases leading to the diffusion difficulty. The effect of Al_2O_3 wt.% on the aluminium reduction peaks in KF-

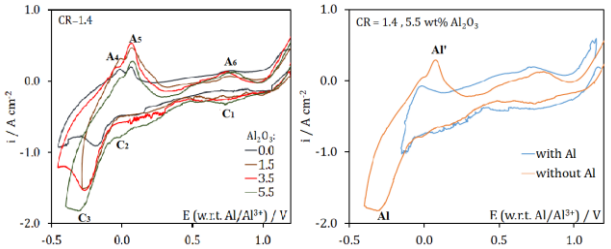

Figure 8. Voltammograms obtained at the W in the KF-AlF_3 melt (CR = 1.4) with varying Al_2O_3 wt% at 800°C dissolved aluminium in the melt with Al_2O_3 of 5.5 wt.% and potential sweep rate of 0.01 V s^{-1}

AlF_3 melts with CR 1.4 is shown in figure 8. With an increase in the Al_2O_3 wt. % in the melt, the cathode and anode region peak tend to increase. The clear peaks on anode and cathode region can be seen, where C_1 is tungsten reduction at 0.7 V (vs. Al). C_2 wave may account to the beginning of the aluminium reduction, which starts from -0.1 V. C_3 corresponding to the aluminium reduction is between -0.2 and -0.25 V depending on the alumina content in the melt. A_4 is related to the dissolution of aluminium from the intermetallic compound Al_4W at -0.1 V. The aluminium oxidation peak A_5 at 0.1 V can be seen, while the tungsten oxidation A6 occurs at 0.75 V.

The values of cathode peak current densities (i_{cp}) and the potentials (E_{cp}) corresponding to i_{cp} for CR (1.3-1.5) and different sweep rates at 800 °C are presented in table 2. The i_{cp} vs. $v^{1/2}$ show linearity for all the cases as shown in figure 9 stating that the process is diffusion controlled. The E_{cp} vs. ln(v) shows that there is a slight shift in the E_{cp} for CR 1.3 and 1.5, meaning that the process is changed from quasi-reversible to diffusion-limited. Although, in melts with CR 1.4, the E_{cp} swift was not seen stating it to be a reversible process. Randles-Sevcik equation (17) can be used to estimate the diffusion coefficient of the electroactive ions to the tungsten cathode as most of the processes are diffusion-controlled [48].

$$i_{cp} = -0.4463(zF)^{3/2}C\left(\frac{vD}{RT}\right)^{1/2} \quad (17)$$

where i_{cp}– cathode peak current density, A cm^{-2}; C – concentration of the electroactive ions, mol cm^{-3}; D – diffusion coefficient of the electroactive ions, cm^2 s^{-1}; v – potential sweep rate, V s^{-1}.

The diffusion coefficient values of the melts with CR's (1.2 to 1.5) lies from 0.028 to 2.724×10^{-5}. It can be observed from table 3 that with an increase in the CR, the D decreases which is in good agreement with Nikolaev et al. [39]. In addition, the D increases with the increase of Al_2O_3 wt.%.

3.2.2 Stationary polarization. Galvanostatic polarization curves were obtained to examine the kinetics of the cathode process on the tungsten electrode in KF-AlF_3 melts to determine the aluminium electrolysis parameters. Typical stationary polarization curves acquired for different CR (1.4 and 1.5) and Al_2O_3 wt.% in melts with CR 1.4 at 800 °C are demonstrated in figure 10. The aluminium reduction takes place closer to the potential of -0.2 V with the cathode limiting current density (i_l) ranging in between 0.45 and 0.5 A.cm^{-2} depending on the [KF/AlF_3] ratio and Al_2O_3 wt.%. The potential at high i_c (between -0.7 and -1.1 V) did not vary much which is associated to the potassium reduction on the cathode and the deposition of the K_3AlF_6 and $KAlF_4$ salts mixture [49].

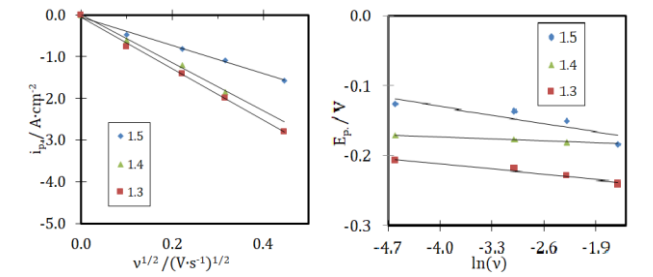

Figure 9. Dependences of $i_{cp}(v^{1/2})$ and $E_{cp}(\ln(v))$ of the aluminium deposition on tungsten electrode in the KF-AlF_3 melt (CR = 1.3 – 1.5 mol mol^{-1}) at 800°C

Limiting currents of 0.45-0.50 A cm^{-2} were observed in melts with CR 1.4 and 1.5. The limiting current of the cathode process increases with the decrease in the CR [40]. This is due to the increase in the diffusion layer thickness associated with a higher proportion of AlF_3. This shows that [KF/AlF_3] ratio plays a key role in the kinetics of the cathode process. The i_l varies between 0.45 and 0.50 A cm^{-2} with increasing Al_2O_3 wt.% from 0.1 to 5.5 %. The absence of proportional increase of i_l with Al_2O_3 content increase in the melts implies that the process was under the mixed kinetics. The same phenomena were observed using the W cathode in melts (CR 1.3) with increasing Al_2O_3 content [40]. Reaction (18) is possible to occur over -0.6 V along with the parallel reaction (19). Segments of electrically conductive $KAlF_4$ and K_3AlF_6 are subjects to form on the surface of the cathode, leading to the passivation.

$$Al + 6KF_{(s)} = K_3AlF_6 + 3K_{(g)} \quad (18)$$

Δ_rG^o (800 °C) = 7.251 kJ.mol^{-1}

$$2Al + AlF_3 = 3AlF \quad (19)$$

Δ_rG^o (800 °C) = -180.876kJ.mol^{-1}

Table 2. Kinetic parameters of aluminium reduction on tungsten in the KF-AlF_3 melts (CR = 1.3-1.5 mol mol^{-1}) at 800°C

$\left[\frac{KF}{AlF_3}\right]$ ratio	υ/V·s^{-1}	$υ^{1/2}$/ (V·s^{-1})$^{1/2}$	ln(υ)	i_{cp}/A·cm^{-2}	E_{cp}/V
1.3	0.01	0.100	-4.605	-0.77	-0.207
	0.05	0.223	-2.995	-1.31	-0.219
	0.10	0.316	-2.302	-2.00	-0.229
	0.20	0.447	-1.609	-2.81	-0.240
1.4	0.01	0.100	-4.605	-0.60	-0.170
	0.05	0.223	-2.995	-1.21	-0.176
	0.10	0.316	-2.302	-1.85	-0.180
	0.20	0.447	-1.609	-	-
1.5	0.01	0.100	-4.605	-0.47	-0.127
	0.05	0.223	-2.995	-0.81	-0.136
	0.10	0.316	-2.302	-1.09	-0.149
	0.20	0.447	-1.609	-1.57	-0.184

Table 3. Diffusion coefficients ($D \cdot 10^5$ / cm^2 s^{-1}) of electroactive ions in KF-AlF_3 melts at 800 °C

$\left[\frac{KF}{AlF_3}\right]$ ratio	$C_{Al(III)}$/mole·cm^{-3}	Al_2O_3 wt. %	$D \cdot 10^5$/$cm^2 \cdot s^{-1}$
1.2	0.00919	0.1	2.724±0.110
1.3	0.00901	0.1	0.104±0.026
1.4	0.00892	0.1	0.081±0.002
1.5	0.00880	0.1	0.040±0.012
1.4	0.00918	1.5	0.488±0.062
1.4	0.00954	3.5	0.474±0.048
1.4	0.00989	5.5	0.624±0.058

Equation (13) is used to calculate the mass transfer coefficients for the set of conditions and is presented in table 4.

Clearly, the mass transfer coefficient increases with increasing CR and alumina content in the melt. While the diffusion layer thickness decreases with an increase in the CR and increases with the increasing alumina content in the melt, which was expected.

3.3 Electrolysis test

3.3.1 Parameters and conditions. The electrolysis parameters were determined based on the stationary parameters and previously obtained results for Cu-Al anode and W cathode working conditions:

□ The limiting current densities for oxygen evolution increased with an increase in CR and T, the anode can perform at a high current density and a rather low overvoltage at CR=1.4 and T=800 °C;

□ KF-AlF_3-Al_2O_3(sat) with CR 1.4 was chosen as the cathode limiting current was almost 0.5 A cm^{-2}. Using CR lower than 1.4 would lead to the K reduction on the cathode and passivation of the cathode with $KAlF_4$ and K_3AlF_6;

□ High alumina solubility and dissolution rate at CR 1.4 at 800°C.

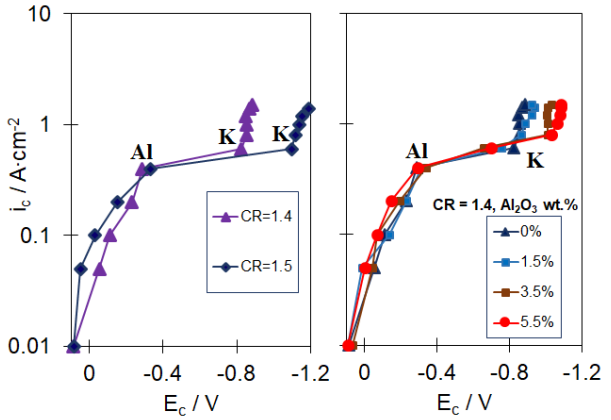

Figure 10. Stationary polarisation curves measured on W electrode at 800°C for CR 1.2-1.5 and varying Al_2O_3 wt.% in melts with CR 1.4

Electrolysis of 1.4KF-AlF_3-Al_2O_3(sat) with the 90Cu-Al anode and wetted tungsten cathode was performed under the following parameters:

- □ current – 10 A
- □ anode current density – 0.25 A cm^{-2}
- □ cathode current density – 0.25 A cm^{-2}
- □ anode-cathode distance – 3 cm
- □ voltage – 3.8–5.8V
- □ temperature – 800°C
- □ duration – 18 hours

The photographs related to the cell along with the cathode and anode used for the electrolysis are shown in figure 11. The gas evolution on the anode was observed during the electrolysis process, assuming the main anode product to be O_2 gas. The anode did not lose its geometry, although an oxide layer was formed on the active surface of the anode (figure 11a). The aluminium reduced was in the form of droplets ranging from 0.1 cm to 4 cm (figure 11c). The tungsten cathode was well wetted with aluminium in the process and no catastrophic corrosion was observed (figure 11d).

The current efficiency of about 84.41 % was obtained. The specific energy consumption for the first four hours was around 14.5 kWh/ kg Al and 19.8 kWh/ kg Al for the last 6 hours. The linearly increasing voltage between the anode and cathode was observed as shown in figure 12. The anodic overvoltage is related to the formation of the fluoride layer between the oxide layer and the Cu-Al alloy. The sudden drop of the potential can be seen (point 2 and 4) which is associated with the depletion of this layer. Oxidation of current leads resulted in the increase of the resistance. In addition, it was observed that the electrical joints were corroded at the end of the electrolysis test. Better protection of current leads and electrical joints can help to reduce the voltage between the anode and cathode.

Table 4. Mass transfer coefficients for diffusion of electroactive particles to the electrode at 800 °C.

$\left[\frac{KF}{AlF_3}\right]$ ratio	Al_2O_3 wt.%	limit current i_l / A cm^{-2}	Mass transfer coefficient $k_s \cdot 10^4/cm^2 \cdot s^{-1}$	Diffusion layer thickness δ/ cm
1.4	0.1	0.45	1.749	0.0044
1.5	0.1	0.45	1.766	0.0020
1.4	1.5	0.47	1.768	0.0276
1.4	3.5	0.48	1.775	0.0273
1.4	5.5	0.50	1.746	0.0358

Note: In this case C is the concentration of Al(III) ions in the melt.

3.3.2 Oxide layer characterization. To have a better understanding of the corrosion mechanism of the anode after an interaction with the melt during the electrolysis, the SEM imaging was performed on the anode at the places where the melt was still present. Figure 13 shows the cross-section of the 90Cu-Al anode after 18-hour electrolysis. With the help of an element-mapping image, it can be seen that the Cu, Al and O elements are evenly distributed in the matrix. While the F element is confined to a single area, which is between the oxide scale and the alloy. The thickness of the entire oxide layer is around 140 µm. The outer layer (≈ 20 µm) is CuO-rich (see zone 2) and surrounded by the electrolyte (see zone 1). The inner layer is about 100 µm, resulted from the inward O diffusion. The oxide layer was composed of CuO, Cu_2O and $CuAlO_2$ according to the atomic ratio obtained from the single point analysis (see zones 3 and 5). This layer also includes phases, which has high concentrations of Cu and O element (see zone 4). A thin layer (≈ 20 µm) comprised of CuF + AlF_3 and CuF_2 + AlF_3 was observed at the surface between the oxide layer and the Cu-rich alloy (see zone 7). Similar metal fluorides were formed between the oxide layer and the alloy in Jucken et al. [50]. A significant amount of Al metal was also present in this particular region; both EDX element mapping and single-point analysis data can validify this statement. The reactions (20) and (21) may occur in this region:

$$Cu_{(s)} + AlF_5^{2-} = CuF_2 + AlF_3 + 2e^- \quad (20)$$

$\Delta_r G^o$ (800 °C) = -367.037 kJ.mol^{-1}

$$Cu_{(s)} + AlF_4^- = CuF + AlF_3 + e^- \quad (21)$$

$\Delta_r G^o$ (800 °C) = -513.279 kJ.mol^{-1}

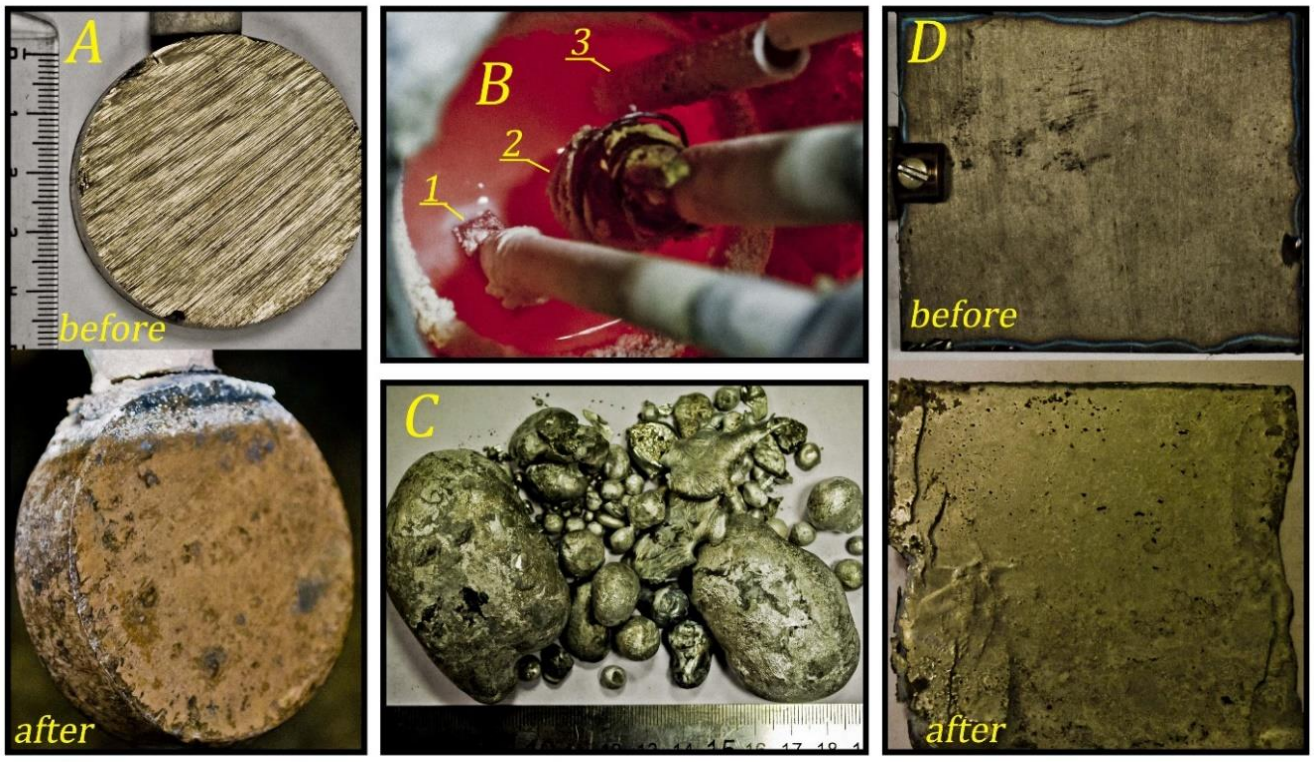

Figure 11. Photos: a. 90Cu-Al anode (before and after the experiment) b. Cell with 1-anode, 2-cathode, 3-thermocouple, c. aluminium produced, d. tungsten cathode (before and after the experiment).

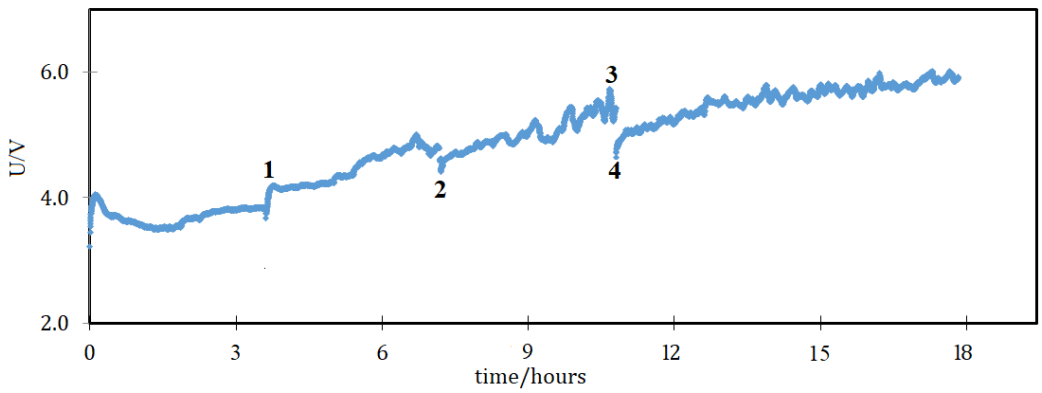

Figure 13. Anode-cathode voltage during the electrolysis for 18 hours with 1.4 KF-AlF_3-Al_2O_3 (sat) melt

The SEM imaging on the outer layer of the anode is shown in figure **Error! Reference source not found.**. The element-mapping image demonstrates that the Cu element is evenly distributed on the outer layer, which establishes that the anode can be electrically conductive even after 18-hour electrolysis. Zone 1 is significantly concentrated with Cu and O elements with 63.28 and 17.10 at.% respectively associated with the presence of Cu element and Cu_2O according to the atomic ratio (see figure 15). It is evident that the Cu present in this area is reduced from the $CuF+AlF_3/CuF_2+AlF_3$, which acts as an electrolyte between the oxide layer and the Cu-Al alloy. The oxide layer acts as a bipolar electrode where it is a cathode towards the Cu-Al anode and as an anode towards the W-Al cathode. While zones 2, 3 and 4 are dominated by F and K elements, meaning the presence of the melt and formation of other complex elements like $KAlF_4$ and K_3AlF_6 and the same complex elements were observed in XRD examination (see figure 16). In zone 5 and 6, the Cu and O elements concentrations are comparatively high, where the Cu_2O and CuO are formed. Table 5 gives a complete understanding of the concentrations of the elements at different places for the SEM-EDX figures 13 and **Error! Reference source not found.**.

The powdered XRD examination of the solidified corrosion layer after the 18-hour electrolysis is shown in figure 16. Three oxide phases were detected from the analysis, Cu_2O, CuO and $CuAlO_2$. The wt. % of the phases are: Cu_2O-27.7%, CuO-30.02%, $CuAlO_2$-13.9%, AlF_3- 3.56%, K_3AlF_6- 9.51%, $KAlF_4$-12.00% and Cu 4.41%. The expected $CuAl_2O_4$ phase was not detected in the examined sample. The Cu element with 4.41

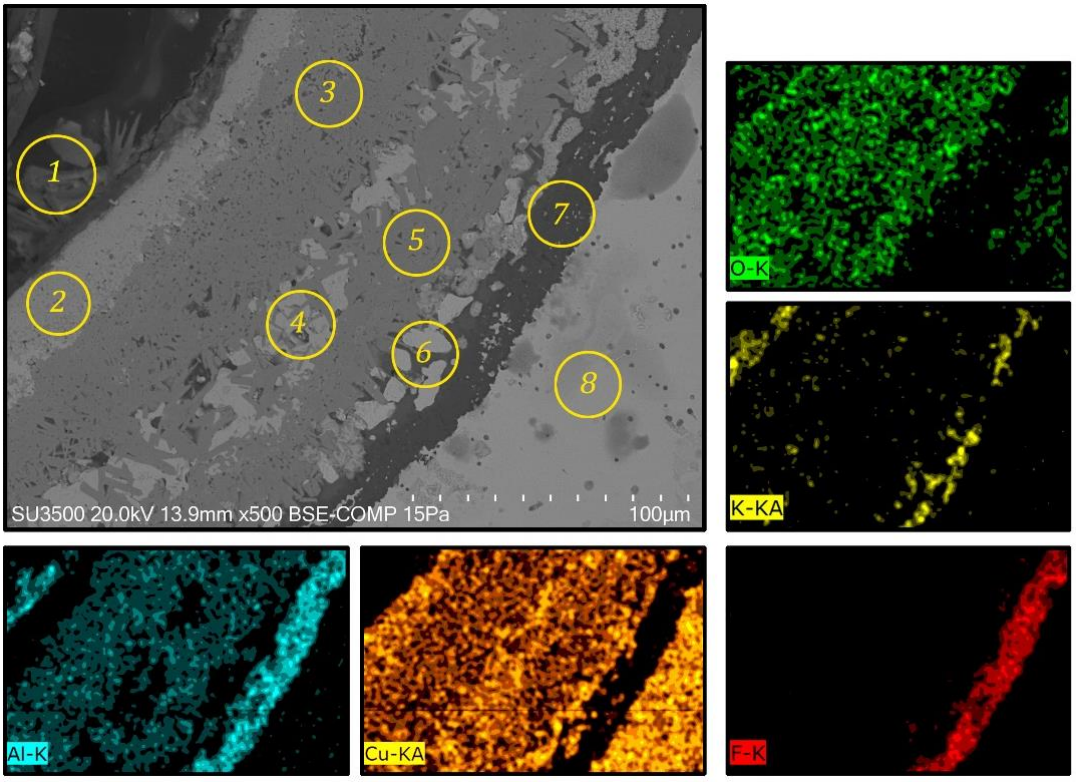

Figure 12. A SEM-EDX image of the cross-section of the 90Cu-Al anode in melt after 18-hour electrolysis.

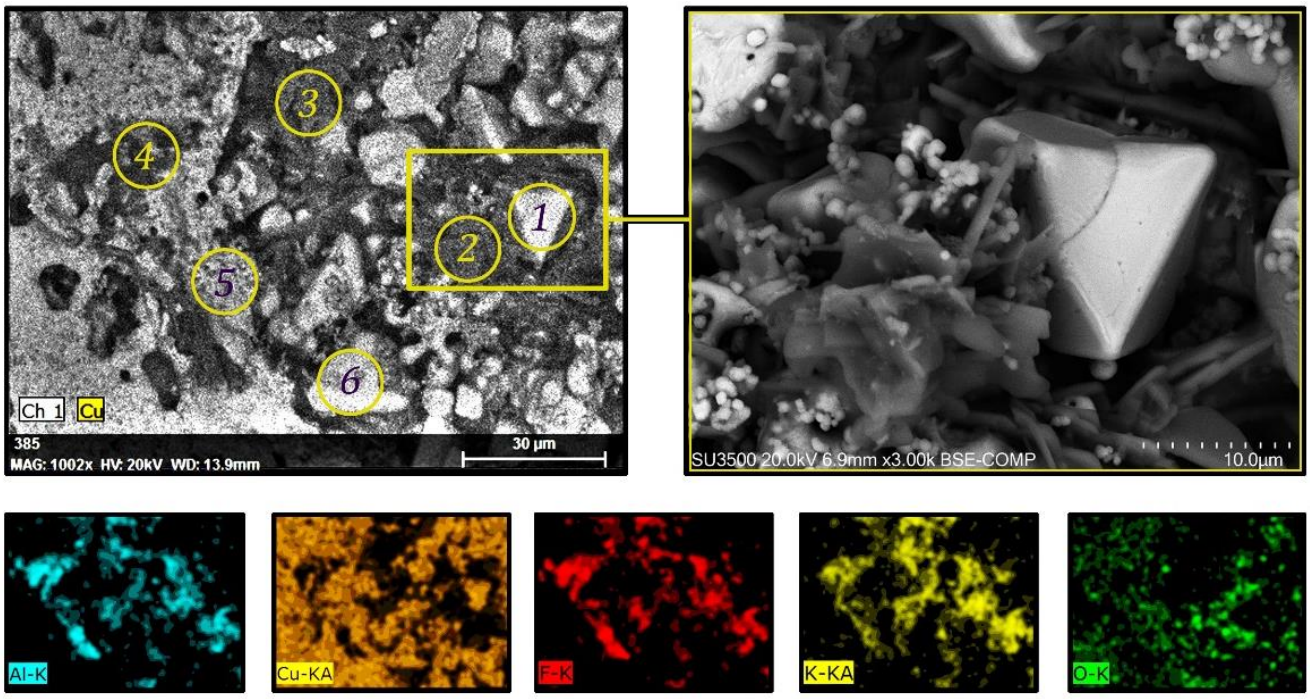

Figure 14. SEM-EDX imaging of the oxide layer on the surface of the 90Cu-Al anode after the electrolysis process

wt.% observed in the oxide powder is formed electrochemically through the Cu ions discharge in the molten fluoride layer between the oxide scale and the anode itself.

3.3.3 Aluminium purity. The composition of the aluminium reduced during electrolysis was analysed using optical emission spectrometer to detect the impurity and the results are shown in table 6. The reduced aluminium contains an acceptable level of impurities. Silicon content of about 0.157% in the metal is acquired form the alumina used in the process and this can be avoided by using smelter grade alumina (SGA) for the reduction process. The Fe content of 0.253% is due to the oxidised current leads and this impurity can be eliminated with proper protection of the current leads and with better anodic geometry. The Cu impurities of 0.0984% in the metal is from the anode. From the obtained electrolysis results, it is clear that the aluminium reduction can be performed using 90Cu-Al anode and wettable cathode with CR 1.4. Higher current efficiencies and metal purity can be attained with minor adjustment using suspension electrolyte and can be adopted to industrial scale in the future.

Annual anode wear rate (WR) can be calculated by using the formula (22)

$$WR = \frac{(m_b.w_b + m_{Al}w_{Al}) \times 365 \times 24}{10^6 \times d_a \times S_a \times t} \quad (22)$$

where m_b is the bath mass (g), m_{Al} is the produced Al mass (g), w_b is the total concentration of Cu contaminants in the bath (ppm), w_{Al} is the total concentration of Cu contaminants in the produced Al in (g), d_a is the density of the 90Cu-Al alloy (g/cc), S_a surface area of the anode, t is time in hours.

The WR of the anode is 0.08 cm/year.

Conclusions

The kinetics of anode and cathode processes was studied in KF-AlF_3 and KF-AlF_3-Al_2O_3 systems with varying CR and temperatures. The electrolysis was carried out based on the results obtained from the investigation of kinetic parameters of electrodes. The main conclusions are as following:

- The mass transfer coefficients for oxygen ions in the anode process increases with increasing CR and T are in the range of 0.5–1.6·10^{-4} cm s^{-2};
- The anodic limiting currents are in the range of 0.3–0.7 A cm^{-2};
- In the cathode process on W electrode, the aluminium deposition on the cathode surface occurs between -0.125 and -0.240 V;
- The peak current densities increase with the decreasing CR's and increasing Al_2O_3 wt.%;
- The processes in melts with CR 1.3 and 1.5 are quasi-reversible to diffusion-limited and with CR 1.4, it is reversible;
- The current efficiency of the electrolysis test was about 84.41%;
- The anode was working without any geometry damage and the wear rate was determined to be 0.08 cm/year;

Table 6. Content of individual elements at.% in the cross-section of the anode and the melts figure 12, and the content on the oxide layer on the surface of the anode in figure **Error! Reference source not found.** using SEM-EDX single-point analysis.

Figure 12 Zone	Cu	Al	O	F	K	Total
1	3.50	14.06	36.27	29.15	27.71	100
2	48.10	4.74	42.98	3.22	0.96	100
3	26.18	21.08	44.47	7.25	1.02	100
4	43.00	19.80	34.92	1.85	0.43	100
5	23.43	25.75	42.76	6.89	1.18	100
6	31.42	21.45	9.17	32.04	5.90	100
7	9.91	19.91	3.74	66.20	0.24	100
8	72.58	13.46	12.30	1.13	0.53	100
Figure **Error! Reference source not found.** Zone	Cu	Al	O	F	K	Total
1	79.18	4.24	6.75	8.01	1.81	100
2	9.70	17.10	7.93	49.06	16.20	100

- From the SEM-EDX, it was found that the oxide scale is about 140 µm thick and the metal fluoride layer of 10 µm was observed in-between the oxide layer and the anode surface. The anode oxide layer acts as a bipolar electrode;
- The cathode aluminium purity was 99.40% and the main impurities were Fe, Si and Cu.

The present results suggest that the aluminium reduction can be performed using 90Cu-Al anode and wettable cathode at CR 1.4 and T=800 °C. Commercial purity aluminium can be produced using SGA and properly protected current leads.

Conflicts of interest

There are no conflicts to declare.

Acknowledgements

The presented study was performed with the financial support of the Russian Science Foundation (Grant No. 19-79-00004).
The authors are grateful to Aleksandr Samoilo, Timofei Bermeshev, Valentin Yanov, Pavel Yuriev for the analysis and materials preparation.

Table 5. Composition of reduced aluminium in electrolysis process.

Element	Al	Si	Fe	Cu	Mn	Mg	Zn
Average	99.40	0.157	0.253	0.0984	0.0070	0.0109	0.0174
S.D	0.029	0.016	0.017	0.0043	0.0004	0.0019	0.0023
Element	Cr	Ni	Ti	Be	Ca	Li	Pb
Average	0.0040	0.0063	0.0005	< 0.0001	> 0.0050	0.0002	0.0031
S.D	0.0002	0.0003	0	0	0.0003	0	0.0011
Element	Sn	Sr	V	Na	Bi	Zr	B
Average	< 0.0005	0.0001	0.0009	< 0.0001	< 0.0025	0.0125	0.0012
S.D	0	0	0.0001	0	0	0.0005	0.0001
Element	Ga	Cd	Co	Hg	In	P	Sc
Average	0.0141	< 0.0005	< 0.0010	< 0.0010	0.0005	< 0.0030	0.0001
SD	0.0005	0	0	0	0.0005	0	0.0001

SD: Standard deviation

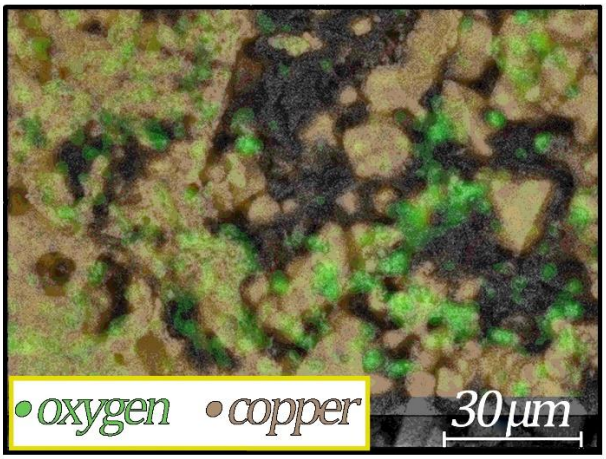

Figure 16. Elemental mapping of oxide layer using SEM-EDX showing the Cu metal dominance.

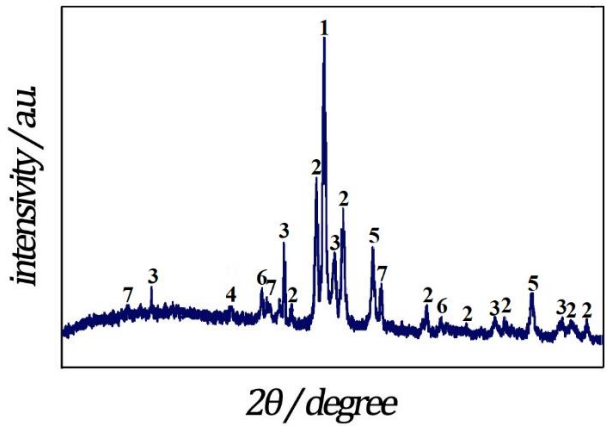

Figure 15. XRD patterns of the reaction layers on the 90Cu-Al anode after 18 hours electrolysis 1-Cu_2O, 2-CuO, 3-$CuAlO_2$, 4- AlF_3, 5- K_3AlF_6, 6- $KAlF_4$, 7- Cu

Notes and references

1. International Aluminium Institute (IAI): Statistics on primary aluminium production. http://www.world-aluminium.org/statistics/. Accessed 02 Jan 2020.
2. G. Saevarsdottir, H. Kvande, B.J. Welch, JOM, 2020, 72(1), 296–308.
3. L. Cassayre, P. Palau, P. Chamelot, L. Massot, J. Chem. Eng. Data, 2010, 55(11), 4549–4560.
4. S.K. Padamata, A.S. Yasinskiy, P.V. Polyakov, Metall. Res. Technol., 2019, 116(4), 410.
5. C.A. McMillan, G.A. Keoleian, Environ. Sci. Technol. 2009, 43(5), 1571–1577.
6. F. Gao, Z. Nie, Z. Wang, H. Li, X. Gong, T. Zuo, Sci. China Ser. E-Tech Sci., 2009, 52(8), 2161–2166.
7. I. Galasiu, R. Galasiu, J. Thonstad, "Inert Anodes for Aluminium Electrolysis", Aluminium-Verlag, 2007, Diisseldorf, 207 p
8. R.P. Pawlek, Light Metals, 2014, 1309–1313
9. H. Kvande, W. Haupin, JOM, 2001, 53 (5), 29–33.
10. D.R. Sadoway, JOM, 2001, 53(5), 34–35.
11. J. Liu, Z. Li, Y. Tao, D. Zhang, K. Zhou, T. Nonferr. Met. Soc. China, 2011, 21 (3), 566–572.
12. M, Glucina, M. Hyland, Light Metals, 2005, 523–528.
13. T. Nguyen, V. de Nora, Light Metals, 2006, 385–390.
14. S. Helle, M. Pedron, B. Assouli, B. Davis, D. Guay, L. Roue, Corros. Sci., 2010, 52(10), 3348–3355.
15. S. Helle, M. Tresse, D. Guay, L. Roue, J. Electrochem. Soc., 2012, 159(4), 62–68.
16. E. Gavrilova, G. Goupil, B. Davis, D. Guay, L. Roue, Light Metals, 2015, 1187–1191.
17. Y.P. Zaikov, VIII. Al Symp., Slovakia, Ziar nad Hronom-Donovaly, 25-27 Sept. 1995, 239–241.
18. G.M. Haarberg G.M. 9th Int. Symp. On Molten Salts, San Francisco, USA, 22-27 May 1994, 568–577.
19. A. Apisarov, A. Dedyukhin, E. Nikolaeva, P. Tinghaev, O. Tkacheva, Al. Redkin, Yu. Zaikov, Metall. Mater. Trans. B., 2010, 42 (1), 236–242.
20. J. Yang, D.G. Graczyk, C. Wunsch, J.N. Hryn, Light Metals, 2007, 537–541.
21. K.P. Trumble, Acta Metall. Mater., 1992, 40 (Suppl.), S105–S110.
22. T. Fujimura, S.I. Tanaka, Acta Mater., 1998, 46 (9), 3057–3061.
23. O.A. Lorentsen, T.E. Jentoftsen, E.W. Dewing, J. Thonstad, Metall. Mater. Trans. B., 2007, 38(5), 833–839.
24. L. Feng, N. Xie, W. Shao, L. Zhen, V.V. Ivanov, J. Alloys Comp., 2014, 610, 214–223.
25. A.S. Yasinskiy, S.K. Padamata, P.V. Polyakov, O.O. Vinogradov, Tsvetnye Metally., 2019, 9, 42–49. (In Russian)
26. A.S. Yasinskiy, S.K. Padamata, P.V. Polyakov, A.S. Suzdaltsev, A.Y.Nikolaev, Light metals, 2020 (In press)
27. M. Sørlie, J. Hvistendahl, H. A. Øye, Light metals, 1993, 921–930.
28. M. Sørlie, H. A. Øye, Cathodes in Aluminium Electrolysis, 3rd edition, Aluminium-Verlag, Dusseldorf, 661 p. (2010).
29. R.P. Pawlek, Light Metals, 2010, 377–382.
30. Q. Li, Y. Lai, J. Li, J. Yang, J. Fang, Z. Chen, Light Metals, 2005, 789–791.
31. Y. Hengwei, L. Wangxing, Q. Shilin, L. Ji, Light Metals, 2010, 855–858.
32. J. Xue, X. Chen, Y. Gao, J. Zhu, Light Metals, 2010, 383–386.
33. X. Lv, C. Guan, Z. Han, C. Chen, J. Mol. Liq., 2019, https://doi.org/10.1016/j.molliq.2019.112017 (In press).
34. S. Bao, K. Tang, A. Kvithyld, T. Engh, M. Tangstad, T. Nonferr. Met. Soc. China, 2012, 22(8), 1930–1938.
35. M. Kontrík, F. Šimko, D. Galusková, M. Nosko, V. Bizovská, M. Hičák, D. Galusek, A. Rakhmatullin, M. Korenko, J. Euro. Cer. Soc., 2018, 38(4), 1143–1151.
36. X. Liao, H.A. Øye, Essent. Read. Light Metals, 2016, 984–991.
37. D. Liu, Zh. Yang, W. Li, S. Wang, and Sh. Wang, J. Solid Stat, Electrochem.,2011, 15, 615-621.
38. D. Liu, Zh. Yang, and W. J. Li, J. Electrochem. Soc., 2010, 157(7), D417-D421.
39. A. Yu. Nikolaev, A. V. Suzdaltsev, P. V. Polyakov, and Yu. P. Zaikova, J. Electrochem. Soc., 2017, 164 (8), H5315–H5321.
40. A. Yu. Nikolaev, A. V. Suzdaltsev, and Yu. P. Zaikov, J. Electrochem. Soc., 2019, 166 (15), D784–D791.
41. Y. Shtefanyuk, V. Mann, V. Pingin, D. Vinogradov, Y. Zaikov, O. Tkacheva, A. Nikolaev, and A. Suzdaltsev, Light Metals, 2015, 589–593.
42. J. Yang, J.N. Hryn, B.R. Davis, A. Roy, G.K. Krumdick, J.A. Pomykala, Jr., Light Metals, 2004, 321–326.
43. J. Yang, J.N. Hryn, G.K. G.K. Krumdick, Light Metals, 2006, 421–424.

44. P.V. Polyakov, A.B. Klyuchantsev, A.S. Yasinskiy, Y.N. Popov, Light Metals, 2016, 283–288.
45. G.A. Gohar, T. Manzoor, A.N. Shah, J. Alloys and Compo., 2018, 735, 802–812.
46. P. Cañizares, J. García-Gómez, I. Fernández de Marcos, M.A. Rodrigo , and J. Lobato , J. Chemi. Edu., 2006, 83 (8), 1204–1207.
47. J. Yang, D.G. Graczyk, C. Wunsch, J.N. Hryn, Light Metals, 2007, 537–541.
48. A. J. Bard and L. R. Faulkner, Electrochemical Methods: Fundamentals and Applications, 2nd edition, N. Y.: John Wiley & Sons Inc., 833 p. (2001).
49. P. S. Pershin, A. V. Suzdaltsev, and Yu. P. Zaikov, J. Electrochem. Soc., 2016, 163 (5), D167–D170.
50. S. Jucken, B. Tougas, B. Davis, D. Guay, L. Roue, Metall. Mater. Trans. B., 2019, 50(6), 3103–3111.

